Implications for an Ionized Alkyl-Enzyme Intermediate during StEH1-Catalyzed *trans*-Stilbene Oxide Hydrolysis†

Lisa T. Elfström and Mikael Widersten*

Department of Biochemistry, BMC, Uppsala University, Box 576, SE-751 23 Uppsala, Sweden

Received September 16, 2005; Revised Manuscript Received November 8, 2005

ABSTRACT: The catalytic mechanism of epoxide hydrolase (EC 3.3.2.3) involves acid-assisted ring opening of the oxirane during the alkylation half-reaction of hydrolysis. Two tyrosyl residues in the active site of epoxide hydrolases have been shown to contribute to the catalysis of enzyme alkylation, but their mechanism of action has not been fully described. We have investigated the involvement of the active site Tyr^{154} and Tyr^{235} during *S,S-trans*-stilbene oxide hydrolysis catalyzed by potato epoxide hydrolase StEH1. Tyr phenol ionizations of unliganded enzyme as well as under pre-steady-state conditions during catalysis were studied by direct absorption spectroscopy. A transient UV absorption, indicative of tyrosinate formation, was detected during the lifetime of the alkyl-enzyme intermediate. The apparent pK_a of Tyr ionization was 7.3, a value more than 3 pH units below the estimated pK_a of protein Tyr residues in the unliganded enzyme. In addition, the pH dependencies of microscopic kinetic rates of catalyzed *S,S-trans*-stilbene oxide hydrolysis were determined. The alkylation rate increased with pH and displayed a pK_a value identical to that of Tyr ionization (7.3), whereas the reverse (epoxidation) reaction did not display any pH dependence. The rate of alkyl-enzyme hydrolysis was inversely dependent on tyrosinate formation, decreasing with its buildup in the active site. Since alkyl-enzyme hydrolysis is the rate-limiting step of the overall reaction, k_{cat} displayed the same decrease with pH as the hydrolysis rate. The compiled results suggested that the role of the Tyr^{154}/Tyr^{235} pair was not as ultimate proton donor to the alkoxide anion but to stabilize the negatively charged alkyl-enzyme through electrophilic catalysis via hydrogen bonding.

The potato epoxide hydrolase (EH)[1] StEH1 (*1*, *2*) belongs to the canonical class of α/*β*-hydrolase fold enzymes (*3*). StEH1 catalyzes hydrolysis of *trans*-stilbene oxide (TSO) according to the scheme illustrated in Figure 1 (*4*). The catalytic mechanisms of EH from various sources have been investigated in detail by mutagenesis (*4*−*7*) and kinetic studies (*4*, *7*−*9*) and by solving three-dimensional structures of enzymes from mammalian (*10*, *11*), microbial (*12*, *13*), and plant sources (*14*). The enzyme active site contains a protein-derived nucleophilic carboxylate group (Asp^{105}; numbering refers to StEH1) which attacks an electrophilic carbon of the bound substrate to form an alkyl-enzyme intermediate (*15*, *16*). Nearby acids (phenols of Tyr^{154} and Tyr^{235}) facilitate ring opening of the oxirane and formation of the alkyl-enzyme (*17*−*20*). The catalytic cycle is concluded by a subsequent nucleophilic attack on the alkyl-enzyme by solvent water, activated by a general base imidazole (His^{300}) followed by release of the diol product (*21*).

The observation that all characterized epoxide hydrolases belonging to the α/*β*-hydrolase fold enzymes contain two tyrosyls has raised the question whether both of these residues are equally important and how they interact.

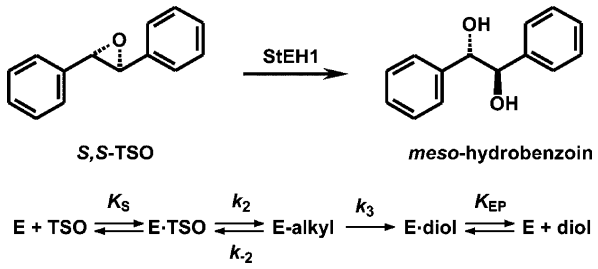

FIGURE 1: Hydrolysis of *S,S-trans*-stilbene oxide (*S,S*-TSO). The catalytic mechanism is divided into two half-reactions of which the initial enzyme alkylation is dependent on enzyme-contributed Tyr acids. The alkyl-enzyme is subsequently hydrolyzed by a base-activated water to release the diol product.

Mutagenesis studies have suggested this to be the case (*4*, *17*−*20*), although it has been proposed from functional studies of Tyr → Phe mutants (*17*), and theoretical calculations (*22*), that only one of the two tyrosyls is required for catalysis of the alkylation step with styrene oxide as substrate. Hence, a definitive function of these residues has not been fully described. One unanswered question has been whether these tyrosyls function as a bona fide Brønstedt acid protonating the leaving group and thus forming a tyrosinate.

The aim of this work was to clarify the role of the active site tyrosyls regarding the nature of acid functionality in connection with structure/function relationships during StEH1-catalyzed hydrolysis of TSO. Data are presented which demonstrate transient tyrosinate formation during hydrolysis of TSO. We propose in concurrence with results reported

† This work was supported by the Carl Trygger Foundation.

* Corresponding author. E-mail: mikael.widersten@biokemi.uu.se. Phone: +46 (0)18 471 4992. Fax: +46 (0)18 55 8431.

[1] Abbreviations: EH, epoxide hydrolase; TSO, *trans*-stilbene oxide; IMAC, immobilized metal ion affinity chromatography; NEPC, *S,S-trans*-3-phenyl-2-oxiranethyl(4-nitrophenyl) carbonate.

10.1021/bi051893g CCC: $33.50
Published on Web 12/13/2005

from a study on the murine soluble enzyme (*18*) that both tyrosyls are required for efficient alkylation and that these residues primarily function as one unit, contributing to hydrogen bonding to the epoxide oxygen.

MATERIALS AND METHODS

Enzyme Isolation. His-tagged wild-type and mutant forms (Y154F, Y235F, and Y154F/Y235F) of StEH1 were expressed and purified as described earlier (*4*). Briefly, the proteins were overexpressed in *Escherichia coli* and purified by a two-step protocol involving Ni(II)-IMAC and size exclusion chromatography. Enzyme concentrations were determined by measuring their intrinsic UV absorbance at 280 nm and applying molar exctinction coefficients calculated from the respective amino acid compositions. Active site titration was performed by detecting the burst formation of 4-nitrophenolate (4NP) after rapid mixing of 5 μM enzyme and 40 μM *S,S-trans*-3-phenyl-2-oxiranethyl(4-nitrophenyl) carbonate (NEPC) in an SX.18MV Sequential stopped-flow spectrophotometer in 0.1 M sodium phosphate, pH 8.0. The concentration of the active enzyme was calculated from $[E]_{\text{active site}} = [4NP]_{\text{burst}}/((k_{\text{obs}}/(k_{\text{obs}} + k_3))^2$ (*23*), where k_{obs} and k_3 are the observed exponential apparent rates of alkyl-enzyme formation and alkyl-enzyme hydrolysis, respectively. Both rates were extracted by following the quenching of intrinsic Trp fluorescence as described previously (*4*); k_{obs} was determined under the same concentration conditions as described above for the 4NP burst formation, while a lower limit value of k_3 was obtained after rapid mixing of 20 μM enzyme with 18 μM NEPC.

Titration of Tyrosinate in Unliganded Enzymes. The ionization behavior of protein Tyr residues, including the proposed catalytic acids Tyr^{154} and Tyr^{235}, was analyzed by UV absorption difference spectroscopy performed in 0.1 M sodium phosphate. Difference spectra for wild-type StEH1−5H and mutants Y154F, Y235F, and Y154F/Y235F (8−15 μM) were recorded in a pH range of 5.5−10.5, using the spectrum recorded at pH 5.5 as reference for zero ionization. The tyrosinate concentration was calculated from the intrinsic absorbance at 295 nm using $\Delta\epsilon = 2.4\ \text{mM}^{-1}\ \text{cm}^{-1}$ (*24*). The structural integrity of the proteins following incubation at extreme pH values was confirmed by subsequent activity measurements in pH 6.8 using the *S,S*-enantiomer of TSO (*S,S*-TSO) as substrate [$\Delta\epsilon = -15\ \text{mM}^{-1}\cdot\text{cm}^{-1}$ for the diol product (*25*)]. *S,S*-TSO was generously provided by Dr. Per I. Arvidsson, Uppsala, Sweden. The pH dependence of the amplitude of the tyrosinate absorbance signal was fitted to eq 1 using the RFFIT program in the SIMFIT package (http://www.simfit.man.ac.uk/) for extraction of the maximal level of ionization and the acid constant.

$$\Delta A_{295} = \frac{\Delta A_{\text{max}}}{1 + [H^+]/K_a} \tag{1}$$

Detection of Tyrosinate during Enzyme-Catalyzed Hydrolysis of S,S-TSO. The transient buildup and disappearance of tyrosinate in the active site during StEH1−5H-catalyzed hydrolysis of *S,S*-TSO was detected under single-turnover conditions (*4*) measuring the UV absorption at 295 nm in a stopped-flow spectrophotometer. The effect of pH on tyrosinate formation was followed in the presence of saturating concentrations of *S,S*-TSO in 0.1 M sodium phosphate and 1% (v/v) acetonitrile between pH 6.5 and pH 8.5 at 30 °C. The tyrosinate concentrations together with the maximal level of tyrosinate formation and the acid constant were calculated as above.

pH Dependence of k_{cat}. Turnover numbers for *S,S*-TSO were determined for mutants Y154F and Y235F from the catalyzed initial rates in the following buffers: pH 5.2−5.7, 0.1 M sodium acetate; pH 6.3−8.8, 0.1 M sodium phosphate; pH 9.5, 0.1 M glycine−NaOH. Equation 2 (*23*) was fitted to the determined k_{cat} values to extract pK_a values. L_H is the pH-dependent parameter (k_{cat}), L_{HA} and L_A are the amounts of the different protonation states of the enzyme−substrate complexes, and K_a is the acid constant.

$$L_H = \frac{L_{HA}[H^+] + L_A K_a}{K_a + [H^+]} \tag{2}$$

pH Dependence of Microscopic Rates. The forward and reverse rates of enzyme alkylation (k_2, k_{-2}) and hydrolysis (k_3) were determined at pH values between 6.5 and 8.5 in the presence of *S,S*-TSO. The reactions were followed in a stopped-flow spectrophotometer at 30 °C in 0.1 M sodium phosphate and 1% (v/v) acetonitrile. The rates of enzyme alkylation and hydrolysis were determined during multiple-turnover and single-turnover conditions, respectively, detecting a transient quenching followed by a recovery of the transient tryptophan fluorescence after passage through a 320 nm cutoff filter as decribed earlier (*4*) or detecting the tyrosinate aborbance signal at 295 nm.

Apparent rate constants were derived by fitting a single exponential, $F = A\ \exp(-k_{\text{obs}}t) + C$, in which A is the amplitude of fluorescence change, k_{obs} the observed rate constant, and C the floating end point of the progression curve (average of 8−14 traces). Kinetic rate constants for steps up to enzyme alkylation were extracted after fitting eq 3 (*25*) using QNFIT in the SIMFIT package. Association/dissociation rates of ES were assumed to be substantially faster than the chemical steps.

$$k_{\text{obs}} = k_{-2} + \frac{k_2[S]}{K_S + [S]} \tag{3}$$

The rate of hydrolysis, k_3, was determined in single-turnover experiments by mixing equimolar amounts of enzyme and substrate (5−10 μM) and following the fluorescence recovery after the alkylation step. k_3 was extracted from $F = A\ \exp(-k_3t) + C$.

Acid constants were extracted by fitting eq 2 to the experimental data with the RFFIT program, where L_H represents the titrated entity (kinetic rates), as described above (*23*).

Structural Comparisons. The structure of 1,8-biphenylenediol was modeled in the program InsightII (Accelrys, San Diego, CA), applying the molecular geometry described by Hine and co-workers (*26*). The atomic coordinates of the active site tyrosyls Tyr^{154} and Tyr^{235} were obtained from the 3-D structure of potato StEH1−5H (*14*). The structures of the tyrosyl pair and 1,8-biphenylenediol were superimposed manually using InsightII.

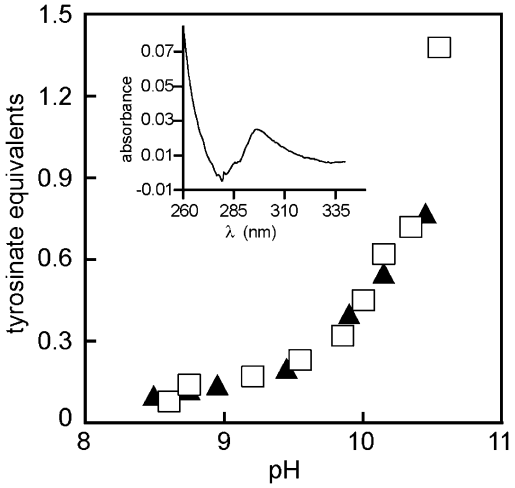

FIGURE 2: Titration of enzyme tyrosyl phenols. No differences in the titration behaviors are observed between the wild-type enzyme (□) and the Y154F/Y235F double mutant (▲), lacking both of the active site tyrosyls. The titration data for the respective single mutants have been omitted from the graph to improve visual clarity. The inset shows a typical difference spectrum of spectra recorded at pH 5.5 subtracted from that recorded at pH 10.1.

RESULTS

Active Site Titrations. The fraction of active enzyme was determined from the burst release of 4-nitrophenol during the first catalytic cycle after rapid mixing of NEPC with StEH1−5H. This compound was chosen over TSO for titration of the enzyme active site, based on the proposed reaction mechanism (*27*) in which 4-nitrophenol is released after enzyme alkylation but prior to hydrolysis. Also, the well-established chromogenic properties of the measured 4-nitrophenol allowed for more accurate determinations of concentration. After compensation for uncomplete deprotonation of released 4-nitrophenol at pH 8.0 (apparent $\Delta\epsilon$ = 12070 M^{-1} cm^{-1}), and introduction of the obtained values of k_{obs} (52 s^{-1}) and k_3 (>19 s^{-1}), the fraction of active enzyme was determined to be >90%.

Acidity of Enzyme Tyrosyl Phenols. Potato StEH1 displays a pH optimum for catalysis of TSO at pH 6.8 (*4*). In order for the active site Tyr^{154} and Tyr^{235} to act as efficient proton donors, they would be expected to be more acidic as compared to typical protein Tyr phenols (pK_a = 9−11). The ionization behaviors of StEH1 Tyr residues, including the proposed catalytic acids Tyr^{154} and Tyr^{235}, were therefore studied. Wild-type StEH1−5H and mutants (Y154F, Y235F, and Y154F/Y235F) (*4*) were analyzed by UV absorption difference spectroscopy at different pH values. A peak at approximately 295 nm, indicative of tyrosinate formation, was observed when subtracting spectra recorded at higher pH values from those recorded at pH 5.5 (inset in Figure 2).

This pH-dependent buildup of tyrosinate in the different enzyme forms allowed for direct titrations and determinations of Tyr acidity in the free enzymes. All four enzyme variants displayed similar titration patterns with estimated pK_a values above 10.5 (Figure 2). The lack of plateau in the plotted titration data suggests that the bulk of tyrosyl phenols were titrated simultaneously and that denaturing conditions would have been required to fully deprotonate all Tyr residues. Hence, none of the tyrosyl phenols (15 in the wild-type enzyme) exhibited unusually acidic pK_a values in the free enzymes.

Detection of Tyrosinate during the Pre Steady State of Catalysis. To analyze possible transient occurrences of deprotonated tyrosyls during catalysis, the formation of tyrosinate was followed directly during single-turnover conditions after mixing of StEH1−5H and *S*,*S*-TSO. A burst increase in absorption at 295 nm, indicative of tyrosinate formation, was evident during the catalyzed reactions with *S*,*S*-TSO. Figure 3 summarizes the obtained results exemplified by data from two different pH values; the buildup of the absorbance signal occurred over the same time period as the enzyme alkylation event (within 200 ms of reaction), followed by measuring quenching of intrinsic Trp fluorescence (Figure 3A). Likewise, the decay of the tyrosinate signal followed the rate of the hydrolytic event, detected as a recovery of the intrinsic tryptophan fluorescence (Figure 3B).

The linkage between Trp fluorescence quenching and tyrosinate formation in epoxide hydrolases has been proposed to be caused by charge transfer between the fluorescing residue and a tyrosinate (*17*). Tyrosinate buildup is also most probably the main source of the observed fluorescence quenching in StEH1; the quenching amplitude decreases with decreased absorance at 295 nm as pH is lowered. A proportion of the quenching, approximately 40% in the reaction with *S*,*S*-TSO, however, cannot be attributed to this effect since it is detected at values of pH where the tyrosinate buildup is insignificant (pH <6.5; data not shown). At present, this residual quenching is viewed as resulting from collisional quenching of Trp^{106} interacting with one of the phenyl groups of bound substrate/intermediate, as suggested from the StEH1 crystal structure (*14*).

The amplitude of the tyrosinate absorbance signal followed a pH dependence which allowed for both determination of the maximal level of formed tyrosinate (i.e., buildup of negative charge) and the acid constant (Figure 4A). Although active site titrations demonstrated that >90% of the enzyme preparation was active, the maximal amplitude achieved with *S*,*S*-TSO as substrate corresponded to approximately 0.4 tyrosinate per enzyme molecule, suggesting that the phenols were not fully deprotonated during alkylation and, hence, did not function as proton donors to the alkoxide oxygen. This includes the assumption that the molar extinction coefficient is not drastically perturbed by substrate binding. The lower than expected tyrosinate signal can also not be directly attributed to microscopic equilibria since the ratios of concentration-determining rates are strongly shifted toward accumulation of the alkyl-enzyme; k_2:k_{-2}:k_3 = 220:38:1, yielding a calculated fraction of 82% of alkyl-enzyme at pH 8.5, as compared to the total concentration of enzyme−substrate complexes. The pK_a value describing the tyrosinate formation (Table 1) suggested that throughout the alkylation step one (or both) of the catalytic tyrosyls is partially ionized and the acidity of the active site Tyr residues is perturbed to a pK_a value more than three pH units below that displayed by the free enzyme.

The active site Tyr residues have been proposed to contribute to catalysis primarily during the alkylation half-reaction of the catalyzed reaction (*7*, *8*, *17*, *18*). Mutating either of these active site tyrosyls into phenylalanyls shifted the rate-limiting step of StEH1-catalyzed hydrolysis of TSO from hydrolysis to alkylation (*4*). Hence, no buildup of the alkyl-enzyme intermediate occurred when either of the single

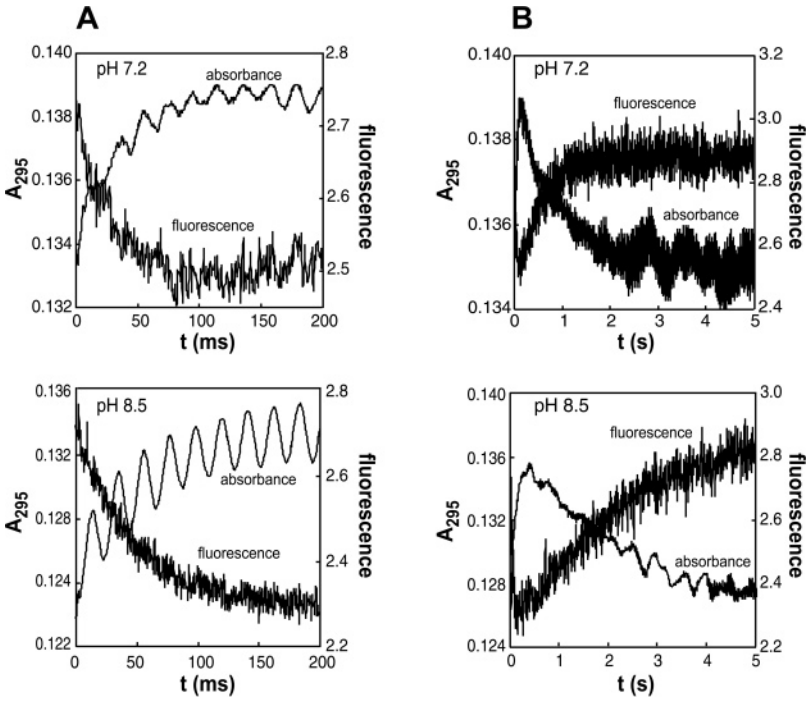

FIGURE 3: Detection of transient buildup and disappearance of tyrosinate in the active site during StEH1−5H-catalyzed hydrolysis of *S*,*S*-TSO. (A) An absorbance signal characteristic of tyrosinate ("absorbance") is detected within the time range (200 ms) of alkyl-enzyme formation. (B) The spectroscopic signal of the tyrosinate disappears with the rate of the hydrolytic half-reaction. The signal of the intrinsic Trp fluorescence (burst decrease followed by a slower recovery phase; "fluorescence") has been included for comparison. Values recorded at pH 7.2 and 8.5 are given as examples. Data were collected as described in the Materials and Methods section. Note: The oscillations of the absorbance signals are due to unsufficiently shielded disturbances of the alternate current field.

Table 1: pH Dependence of Tyr Ionization and Catalytic Rates of *S*,*S*-TSO Hydrolysis

	pK_a					
enzyme	tyrosyls	k_2 (s^{-1})	k_{-2} (s^{-1})	k_3 (s^{-1})	k_{cat} (s^{-1})	tyrosinate (equiv)[a]
wild type	7.3 ± 0.2	7.3 ± 0.2	pH independent	7.4 ± 0.2	5.0 ± 0.2/7.3 ± 0.2[b]	0.4 ± 0.02
Y154F					6.0 ± 0.2/−[c]	
Y235F					6.0 ± 0.2/−[c]	

[a] Tyrosinate per enzyme molecule, calculated from the maximal amplitude of the tyrosinate signal. [b] Data for the wild-type enzyme were adapted from ref *4*. [c] Only the acidic limb of the titration curve is present.

Y154F or Y235F mutants was analyzed during the pre steady state of catalysis, and any possible tyrosinate buildup escaped detection (data not shown).

pH Dependence of Catalytic Rates. To assess a possible linkage between the pH dependence of the active site Tyr residues with catalysis, the rates of alkylation (k_2), intramolecular epoxidation (k_{-2}), and alkyl-enzyme hydrolysis (k_3) during catalyzed hydrolysis of *S*,*S*-TSO were determined at varying values of pH (Figure 4A,B). The alkylation rate increased with pH with a pK_a indistinguishable from that of tyrosyl ionization (Table 1), whereas the rate for the reverse reaction (k_{-2}) was virtually unaffected by pH within the tested range (Figure 4A). Hydrolysis of the alkyl-enzyme (k_3), however, decreased with pH also displaying a pK_a identical to that of tyrosyl ionization (Figure 4B, Table 1).

The basic limb of the pH profile of k_{cat}, of the wild-type enzyme, mimicked the titration of k_3, confirming alkyl-enzyme hydrolysis as the rate-limiting step of product diol formation (*4*). When the respective single mutants were studied, the requirement for the presence of both Tyr^{154} and Tyr^{235} became evident; the turnover numbers with *S*,*S*-TSO decreased in these mutants by 2−3 orders of magnitude depending on the assay pH. Both mutants displayed similar pH dependencies titrating with only one pK_a at an acidic pH (Figure 4C, Table 1), most likely mirroring deprotonation of the catalytic His^{300} in its imidazolium form.

DISCUSSION

Role of the Tyr^{154}/Tyr^{235} Pair. The StEH1−5H-catalyzed alkylation half-reaction involves a nucleophilic attack by the Asp^{105} carboxylate on one of the TSO oxirane carbons in which the charge of the nucleophile is transferred to the epoxide oxygen. Facilitation of oxirane ring opening through satisfaction of the resulting excess electron density of the epoxide oxygen may be achieved either by protonation through general acid catalysis or by stabilization of the resulting alkoxide anion through electrophilic catalysis. Both of these possibilities were considered throughout this study with the experimental results interpreted as discussed below.

A direct proton transfer from one of the active site Tyr residues would require a perturbed, more acidic, pK_a of the phenol group to ensure efficient protonation. The titration data, however, did not indicate that any of the Tyr residues in StEH1−5H possessed unusual acidity in the unliganded enzyme (Figure 2). Hence, for efficient proton transfer to occur, a large pK_a perturbation caused by binding of substrate

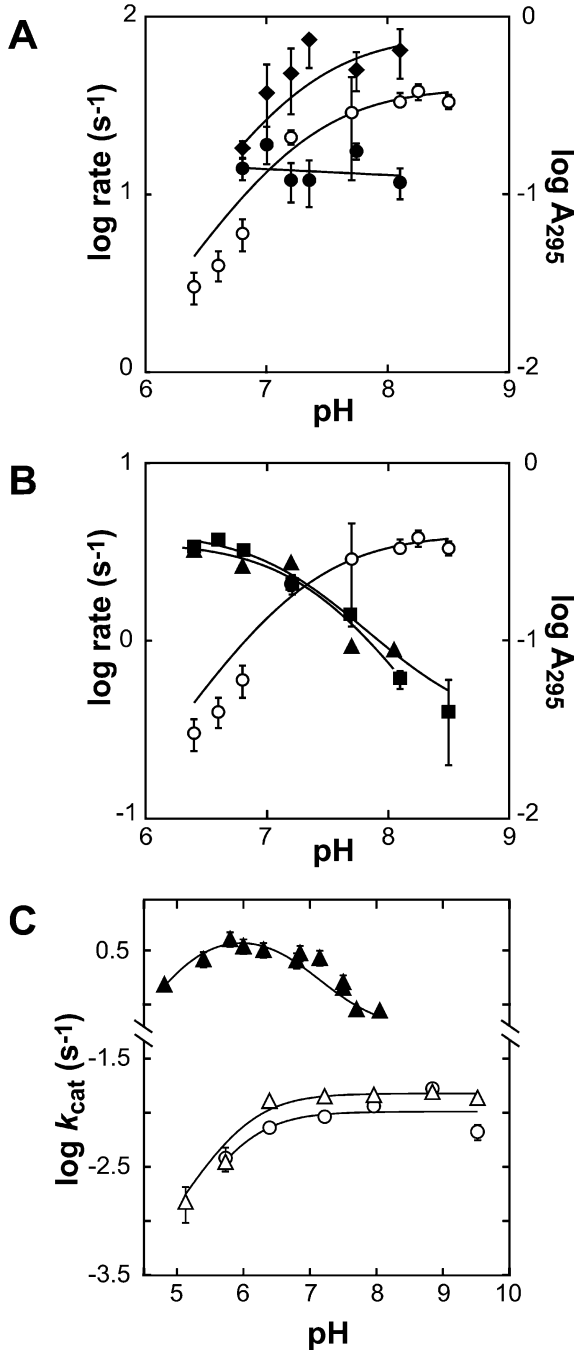

FIGURE 4: (A) pH dependence of tyrosinate formation and catalytic rates for the first half-reaction. The titrated Tyr phenol (○) displays a pK_a value of 7.3 (±0.2) and a maximal ionization corresponding to approximately 0.4 tyrosinate per enzyme molecule. The kinetic rate of alkylation, k_2 (◆), increases with pH to a plateau above pH 7.5 with a pK_a value identical to that for tyrosinate buildup. The rate of the reverse reaction, k_{-2} (●), however, appears virtually unaffected by changes in pH within the tested range. (B) Effects of tyrosinate buildup and pH on the hydrolytic half-reaction. The rates of alkyl-enzyme hydrolysis, k_3 (■) and k_{cat} (▲), both titrate with pK_a values indistinguishable from that of the tyrosinate buildup (○). In contrast to k_2, the rate of hydrolysis (and k_{cat}) decreases with increasing pH. Bars represent the standard error of plotted values. (C) pH dependence of k_{cat} in the Y154F (△) and Y235F (○) mutants. Both mutants titrate with a single acidic pK_a lacking the basic limb of the pH profile displayed by the wild-type enzyme (▲).

or reaction intermediates had to be invoked. The detected absorption signal, indicative of tyrosinate formation, present only during the alkylation half-reaction could indeed support this notion (Figure 3). The pH dependencies of the microscopic reaction rates, however, contradicted a model of general acid catalysis; the rate of alkyl-enzyme formation (k_2 in Figure 1) increased with pH (Figure 4), displaying a pK_a value identical to that of tyrosinate (Tyr ionization) formation (7.3 ± 0.2). If a general acid mechanism had predominated, the pH dependence of k_2 would be expected to follow that of an acid titration, with a decreasing rate at higher pH values as the acid is deprotonated. Therefore, our working model is that the observed pH dependence of k_2 reflects the acidity of the conjugate acid (the alcohol) of the epoxide leaving group alkoxide, with the active site tyrosyls stabilizing the formed oxyanion by donating accessible molecular orbitals through hydrogen bond interactions. In this mechanism, the detected absorption signal is being interpreted as resulting from a *transient hydrogen-bonded tyrosinate* in which full proton transfer to the alkoxide has not occurred and the negative charge is delocalized; the phenol protons are shared between the Tyr^{154}/Tyr^{235} pair and the alkoxide anion. Similar tyrosinate species, which display spectral properties intermediate to those of fully protonated or deprotonated tyrosyls, have been observed in other systems such as calmodulin (*28*) and photosystem II (*29*).

This proposed role of the Tyr pair would require the pK_a of the 1,2-diphenyl-1-ethyl ester 2-hydroxy intermediate to be lowered from an estimated value of 13.5 in solution (pK_a calculator, Marvin; ChemAxon Ltd.) to 7.3 through stabilizing interactions in the active site. An estimate of the required energy contribution from the catalyst corresponds to approximately 36 kJ/mol at 30 °C (as calculated from the respective acid constants). This value is on par with computer simulations of contributed stabilization energies of oxyanionic intermediates in other hydrolytic enzymes (*30*, *31*). Since the rate-limiting step of the overall epoxide conversion was shifted from alkyl-enzyme hydrolysis in the wild-type enzyme to its formation in the Y154F and Y235F mutants, the drastically decreased turnover numbers displayed by these mutants are a likely reflection of a loss in required stabilizing interactions caused by these replacements.

The postulated presence of a stabilized oxyanion intermediate is further supported by the pH profile of the rate of the reverse intramolecular epoxidation reaction (k_{-2} in Figure 1). This reaction is expected to proceed through nucleophilic attack by the alkoxide with the Asp^{105} carboxylate as the leaving group to close the epoxide ring. The observation that the rate of this reaction, k_{-2}, is in large unaffected by pH within the tested range (Figure 4A) indicates that the reverse epoxidation reaction occurs prior to protonation of the alkoxide intermediate, resulting in a maintained reactivity over the tested pH range.

Proton Donor. The excess electron density on the active site Tyr pair when in complex with the oxyanion would be expected to increase the basicity of the phenols. A more basic character may facilitate proton transfer from water to the epoxide oxyanion. The invoked presence of a catalytic water participating in the alkylation half-reaction is in agreement with the solved three-dimensional structure of StEH1−5H (*14*), in which a chain of water molecules connects the solvent with the hydroxyl group of Tyr^{154}. The rate of alkoxide protonation is presumably too rapid to be detected within the time scale of the stopped-flow apparatus; i.e., subsequent hydrolysis and decrease of the tyrosinate signal

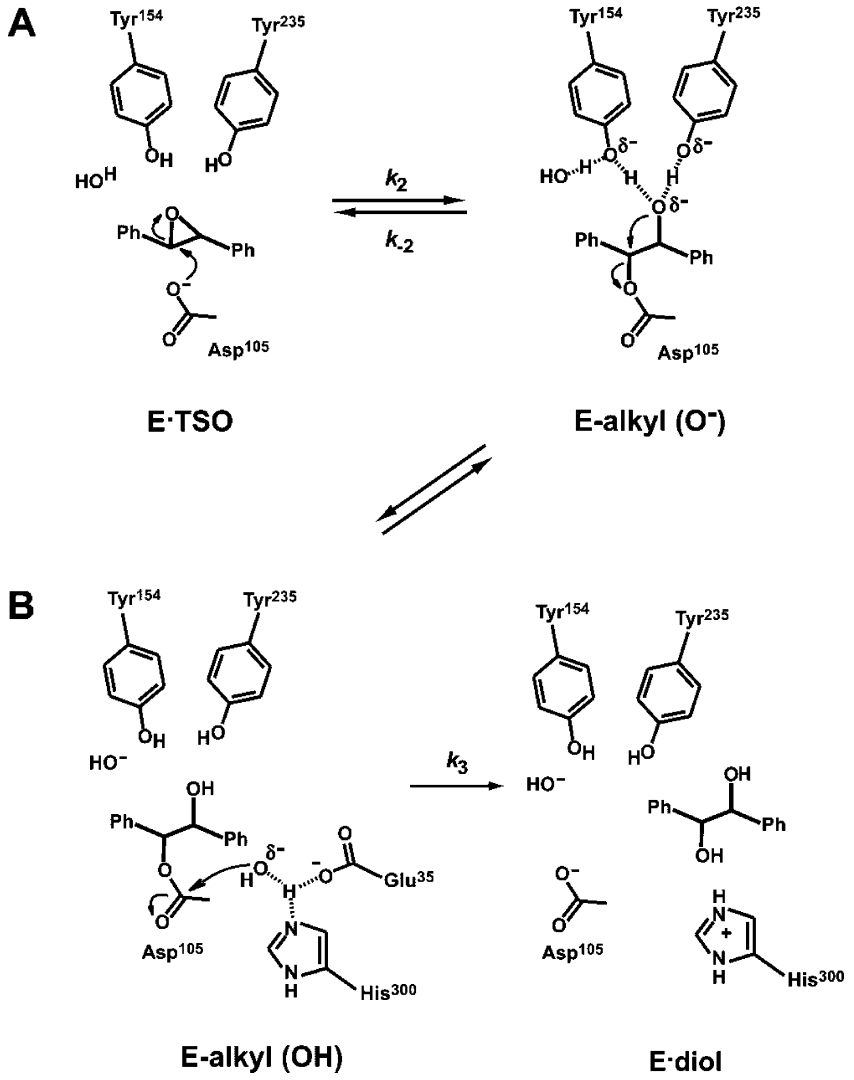

FIGURE 5: Proposed mechanism based on the kinetic properties of StEH1. (A) The Tyr^{154}/Tyr^{235} phenols facilitate epoxide ring opening by accepting the excess electronic charge on the leaving group oxygen originating from the incoming Asp^{105} carboxylate nucleophile. In the proposed formed anionic alkyl-enzyme intermediate ("E-alkyl") no complete proton transfer has occurred. The reverse reaction (with rate k_{-2}) is facilitated by the stabilization of the deprotonated form of the enzyme adduct. The mechanism invokes a catalytic water which serves both for the purpose of stabilizing the alkyl-enzyme and as a proton donor prior to the subsequent hydrolytic step. (B) The protonated alkyl-enzyme decomposes as a result of nucleophilic attack by a water activated by His^{300} [in combination with Glu^{35}, as judged from analysis of the 3-D structure (*14*)]. Dotted lines indicate hydrogen bonds.

are detected as occurring simultaneously. The protonation step may be invoked, however, to occur prior to hydrolysis of the alkyl-enzyme due to the otherwise dianionic, and unfavorable, nature of the resulting tetrahedral intermediate. Figure 5 outlines a proposed mechanism of the enzyme-catalyzed reaction in which the stabilized anionic alkyl-enzyme intermediate [E-alkyl (O^-)] involves the two active site tyrosyls hydrogen bonded to the enzyme−alkoxide adduct and to one solvent water.

Hydrolysis of the Alkyl-Enzyme. We have previously demonstrated that a reaction step downstream of formation of the ionized alkyl-enzyme is rate limiting in StEH1−5H hydrolysis of TSO (*4*), the current view being that subsequent steps involve the rate-limiting hydrolysis (k_3 in Figure 1) followed by rapid product release. It is evident from the present data that the pH dependencies of k_3 and k_{cat} are inversely related to the ionization of the active site tyrosyls. The hydrolysis rate (and k_{cat}) decreases at pH values over 6.5 (Figure 4B). The pK_a values for the decrease in k_{cat} and k_3 are in agreement with the pK_a for tyrosinate formation (Table 1). This somewhat contradicts the expected behavior for hydrolysis of an ester by an activated water (hydroxide ion) which is assumed to be facilitated at higher pH values. One plausible explanation for the pH-dependent rate decrease, as discussed above, is that buildup of negatively charged alkyl-enzyme in the active site at higher pH would increase the activation energy for the likewise negatively charged transition state of hydrolysis by unfavorable electrostatic interactions, lowering the overall hydrolysis rate. Such a behavior would be analogous to other diprotic acids.

Structural Considerations. It has previously been suggested that the tyrosyl pair acts as a general acid catalyst donating a proton to the oxirane oxygen, with the formed tyrosinate being stabilized through hydrogen bonding to the neighboring tyrosyl phenol (*17*). Such a mechanism would require the two phenol groups to be located at a distance close enough for hydrogen bonding to take place or that flexibility and movement in the lid domain of the protein (*3*) would allow the Tyr phenols to be positioned at hydrogen-bonding distance. This has, however, not been exemplified in any of

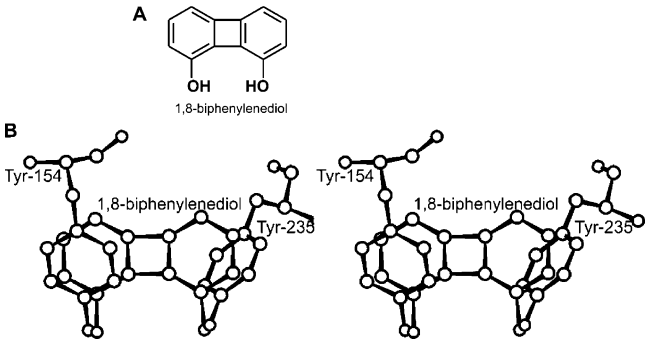

FIGURE 6: (A) Structure of 1,8-biphenylenediol, an efficient catalyst of epoxide ring opening. (B) Stereo image. The structure of the tyrosyl pair in the active site of StEH1 resembles that of 1,8-biphenylenediol. The positioning of the electrophilic phenols in 1,8-biphenylenediol is similar to that of the tyrosyl pair in the active site of StEH1−5H.

the epoxide hydrolases of known structure, in which the distances separating the phenolic oxygens range from 4.4 to 5.4 Å (*10*−*14*). A stabilizing interaction would require a bridging atom provided either by solvent water or by the alkyl-enzyme. If, however, the role of the tyrosyl pair was to function as one bidentate unit accepting electrons from the nucleophilic oxirane oxygen, the positioning of the phenol groups appears well suited.

Site-Directed Mutagenesis. It can be concluded from available structure data and sequence alignments that all established epoxide hydrolases belonging to the α/*β*-hydrolase fold family contain two active site tyrosyl residues. The mutual importance of both tyrosyls has been established from mutagenesis studies, both on the StEH1−5H enzyme and on the murine-soluble EH (*18*). The catalytic efficiencies of the respective single mutants of StEH1−5H with *S*,*S*-TSO, as measured by k_{cat}/K_m, were 0.02% (Y154F) and 0.06% (Y235F), respectively, as compared to the wild-type enzyme (at pH 6.8). These values translate to transition state destabilizations of 21 (Y154F) and 19 (Y235F) kJ/mol in these mutants. The decrease appears to be mainly due to a lowering of the alkylation rate manifested as a 300-fold decrease in k_{cat}, probably directly reflecting poorer stabilization of the high-energy alkyl-enzyme intermediate in these mutants.

A Bidentate Acid in the Active Site of Epoxide Hydrolases? As pointed out by Blée and co-workers, the active site tyrosyls of epoxide hydrolases share characteristics of bidentate phenolic acids such as 1,8-biphenylenediol (*20*) (Figure 6A). This compound has been shown to catalyze epoxide ring opening with an efficiency exceeding that expected from its acid constant (*32*). In a computer-simulated aminolysis of ethyl oxide, the transfer of negative charge from the incoming nucleophile to the acid was less than one unit, demonstrating that 1,8-biphenylenediol acts by electrophilic catalysis (*33*). The catalytic effect afforded by the acid is proposed to be primarily due to removal of electronic charge on the epoxide oxygen. This is more efficiently achieved since two well-aligned unoccupied molecular orbitals are provided. Comparing the structures of the tyrosyl pair in StEH1−5H with that of 1,8-biphenylenediol (*26*), large similarities in topology and orientation of the phenol groups are obvious (Figure 6B). It appears from the present results that not only the structural but also functional features may be similar between the tyrosyl pair of StEH1 and 1,8-biphenylenediol; the apparent roles as electrophilic catalysts harboring excess electron charge in high-energy reaction species.

CONCLUSIONS

The presence of a catalytic acid in the first alkylation half-reaction in epoxide hydrolase catalysis was invoked from early investigations on these enzymes (*6*, *34*). The reaction involves nucleophilic addition of an Asp carboxylate to one of the oxirane carbons, and the catalytic role of the acid would be to facilitate oxirane ring opening by satisfying the buildup of electronic charge on the epoxide oxygen.

When the first three-dimensional structure of an epoxide hydrolase was determined, it became evident that the acid role was played by a pair of Tyr residue phenols (*12*). These tyrosyls have subsequently been confirmed as evolutionarily conserved in all characterized epoxide hydrolases (*35*), and their functional importance has been established from mutagenesis studies. It has not been clear, however, whether both of the tyrosyls are required for catalysis or if there are other, e.g., structural, reasons for the presence of the tyrosyl pair. Although the function of the Tyr phenol(s) has been invoked as a general acid proton donor (*17*−*20*), this has not been firmly established.

We have through site-directed mutagenesis established the Tyr^{154}/Tyr^{235} pair in StEH1−5H as the residues being ionized during the alkylation half-reaction of aromatic epoxide hydrolysis. The determined ionic states of these Tyr phenols at different pH values, combined with kinetic data, point toward a function for the Tyr^{154}/Tyr^{235} pair of StEH1 as hydrogen bond donors. The findings that the rate of the acid-catalyzed alkylation half-reaction displays a pH dependence of a catalytic base and that the buildup of tyrosinate at saturating substrate concentrations is less than half unit charge per active site do not favor a role as a general acid catalyst. Although circumstantial, it becomes intriguing to speculate that the structural feature of a pair of Tyr residues in the active site of epoxide hydrolases has evolved to harness the same catalytic features otherwise found in compounds such as 1,8-biphenylenediol.

ACKNOWLEDGMENT

The generous contribution from Dr. Per I. Arvidsson, Department of Chemistry, Uppsala University, Sweden, to this study is gratefully acknowledged.

REFERENCES

1. Stapleton, A., Beetham, J. K., Pinot, F., Garbarino, J. E., Rockhold, D. R., Friedman, M., Hammock, B. D., and Belknap, W. R. (1994) Cloning and expression of soluble epoxide hydrolase from potato, *Plant J. 6*, 251−258.
2. Morisseau, C., Beetham, J. K., Pinot, F., Debernard, S., Newman, J. W., and Hammock, B. D. (2000) Cress and potato soluble epoxide hydrolases: purification, biochemical characterization, and comparison to mammalian enzymes, *Arch. Biochem. Biophys. 378*, 321−332.
3. Ollis, D. L., Chea, E., Cygler, M., Dijkstra, B., Frolow, F., Franken, S. M., Harel, M., Remington, S. J., Silman, I., Schrag, J., Sussman, J. L., Verschueren, K. G. H., and Goldman, A. (1992) The α/*β* hydrolase fold, *Protein Eng. 5*, 197−211.
4. Elfström, L. T., and Widersten, M. (2005) Catalysis of potato epoxide hydrolase, StEH1, *Biochem. J. 290*, 633−640.
5. Pinot, F., Grant, D. F., Beetham, J. K., Parker, A. G., Borhan, B., Landt, S., Jones, A. D., and Hammock, B. D. (1995) Molecular

and biochemical evidence for the involvement of the Asp-333−His-523 pair in the catalytic mechanism of soluble epoxide hydrolase, *J. Biol. Chem. 270*, 7968−7974.
6. Arand, M., Wagner, H., and Oesch, F. (1996) Asp333, Asp495, and His523 form the catalytic triad of rat soluble epoxide hydrolase, *J. Biol. Chem. 271*, 4223−4229.
7. Rink, R., Fennema, M., Smids, M., Dehmel, U., and Janssen, D. B. (1997) Primary structure and catalytic mechanism of the epoxide hydrolase from *Agrobacterium radiobacter* AD1, *J. Biol. Chem. 272*, 14650−14657.
8. Laughlin, L. T., Tzeng, H. F., Lin, S., and Armstrong, R. N. (1998) Mechanism of microsomal epoxide hydrolase. Semifunctional site-specific mutants affecting the alkylation half-reaction, *Biochemistry 37*, 2897−2904.
9. Tzeng, H.-F., Laughlin, L. T., and Armstrong, R. N. (1998) Semifunctional site-specific mutants affecting the hydrolytic half-reaction of microsomal epoxide hydrolase, *Biochemistry 37*, 2905−2911.
10. Argiriadi, M. A., Morisseau, C., Hammock, B. D., and Christianson, D. W. (1999) Detoxification of environmental mutagens and carcinogens: structure, mechanism, and evolution of liver epoxide hydrolase, *Proc. Natl. Acad. Sci. U.S.A. 96*, 10637−10642.
11. Gomez, G. A., Morisseau, C., Hammock, B. D., and Christianson, D. W. (2004) Structure of human epoxide hydrolase reveals mechanistic inferences on bifunctional catalysis in epoxide and phosphate ester hydrolysis, *Biochemistry 43*, 4716−4723.
12. Nardini, M., Ridder, I. S., Rozeboom, H. J., Kalk, K. H., Rink, R., Janssen, D. B., and Dijkstra, B. W. (1999) The X-ray structure of epoxide hydrolase from *Agrobacterium radiobacter* AD1. An enzyme to detoxify harmful epoxides, *J. Biol. Chem. 274*, 14579−14586.
13. Zou, J., Hallberg, B. M., Bergfors, T., Oesch, F., Arand, M., Mowbray, S. L., and Jones, T. A. (2000) Structure of *Aspergillus niger* epoxide hydrolase at 1.8 Å resolution: implications for the structure and function of the mammalian microsomal class of epoxide hydrolases, *Struct. Folding Des. 8*, 111−122.
14. Mowbray, S., Elfström, L. T., Ahlgren, K. M., Andersson, C. E., and Widersten, M. (2005) X-ray structure of potato epoxide hydrolase sheds light on its substrate specificity, *Protein Sci.* (in press).
15. Lacourciere, G. M., and Armstrong, R. N. (1993) The catalytic mechanism of microsomal epoxide hydrolase involves an ester intermediate, *J. Am. Chem. Soc. 115*, 10466−10467.
16. Borhan, B., Jones, D. A., Pinot, F., Grant, D. F., Kurth, M. J., and Hammock, B. D. (1995) Mechanism of soluble epoxide hydrolase, *J. Biol. Chem. 270*, 26923−26930.
17. Rink, R., Kingma, J., Lutje Spelberg, J. H., and Janssen, D. B. (2000) Tyrosine residues serve as proton donor in the catalytic mechanism of epoxide hydrolase from *Agrobacterium radiobacter*, *Biochemistry 39*, 5600−5613.
18. Yamada, T., Morisseau, C., Maxwell, J. E., Argiriadi, M. A., Christianson, D. W., and Hammock, B. D. (2000) Biochemical evidence for the involvement of tyrosine in epoxide activation during the catalytic cycle of epoxide hydrolase, *J. Biol. Chem. 275*, 23082−23088.
19. Argiriadi, M. A., Morisseau, C., Goodrow, M. H., Dowdy, D. L., Hammock, B. D., and Christianson, D. W. (2000) Binding of alkylurea inhibitors to epoxide hydrolase implicates active site tyrosines in substrate activation, *J. Biol. Chem. 275*, 15265−15270.
20. Blée, E., Summerer, S., Flenet, M., Rogniaux, H., Van Dorsselaer, A., and Schuber, F. (2005) Soybean epoxide hydrolase. Identification of the catalytic residues and probing of the reaction mechanism with secondary kinetic isotope effects, *J. Biol. Chem. 280*, 6478−6487.
21. Tzeng, H.-F., Laughlin, L. T., Lin, S., and Armstrong, R. N. (1996) The catalytic mechanism of microsomal epoxide hydrolase involves reversible formation and rate-limiting hydrolysis of the alkyl-enzyme intermediate, *J. Am. Chem. Soc. 118*, 9436−9437.
22. Lau, E. Y., Newby, Z. E., and Bruice, T. C. A. (2001) Theoretical examination of the acid-catalyzed and noncatalyzed ring-opening reaction of an oxirane by nucleophilic addition of acetate. Implications to epoxide hydrolases, *J. Am. Chem. Soc. 123*, 3350−3357.
23. Fersht, A. (1999) *Structure and mechanism in protein science*, pp 169−173, W. H. Freeman, New York.
24. Glazer, A. N. (1976) The chemical modification of proteins by group-specific and site-specific reagents, in *The Proteins* (Neurath, H., and Hill, R. L., Eds.) 3rd ed., Vol. 2, pp 1−103. Academic Press, New York.
25. Wixtrom, R. N., and Hammock, B. D. (1988) Continuous spectrophotometric assays for cytosolic epoxide hydrolase, *Anal. Biochem. 174*, 291−299.
26. Hine, J., Kyunghyem A., Gallucci, J. C., and Linden S.-M. (1990) Structures of double-hydrogen-bonded adducts of 1,8-biphenylenediol and related compounds, *Acta Crystallogr. C46*, 2136−2146.
27. Dietze, E. C., Kuwano, E., and Hammock, B. D. (1994) Spectrophotometric substrates for cytosolic epoxide hydrolase, *Anal. Biochem. 216*, 176−187.
28. Pundakt, S., and Roche, R. S. (1984) Tyrosine and tyrosinate fluorescence of bovine testes calmodulin: calcium and pH dependence, *Biochemistry 23*, 1549−1555.
29. Haumann, M., Mulkidjanian, A., and Junge, W. (1999) Tyrosine-Z in oxygen-evolving photosystem II: a hydrogen-bonded tyrosinate, *Biochemistry 38*, 1258−1267.
30. Ishida, T., and Kato, S. (2003) Theoretical perspectives on the reaction mechanism of serine proteases: the reaction free energy profiles of the acylation process, *J. Am. Chem. Soc. 125*, 12035−12048.
31. Hermann, J. C., Hensen, C., Ridder, L., Mulholland, A. J., and Höltje, H.-D. (2005) Mechanisms of antibiotic resistance: QM/MM modeling of the acylation reaction of a class A β-lactamase with benzylpenicillin, *J. Am. Chem. Soc. 127*, 4454−4465.
32. Hine, J., Linden, S.-M., and Kanagasabapathy, V. M. (1985) Double-hydrogen-bonding catalysis of the reaction of phenyl glycidol ether with diethylamine by 1,8-biphenylenediol, *J. Org. Chem. 50*, 5096−5099.
33. Omoto, K., and Fujimoto, H. (2000) Theoretical study of activation of oxirane by bidentate acids, *J. Org. Chem. 65*, 2464−2471.
34. Bell, P. A., and Kasper, C. B. (1993) Expression of rat microsomal epoxide hydrolase in *Escherichia coli*. Identification of a histidyl residue essential for catalysis, *J. Biol. Chem. 268*, 14011−14017.
35. Armstrong, R. N., and Cassidy, C. S. (2000) New structural and chemical insight into the catalytic mechanism of epoxide hydrolases, *Drug Metab. Rev. 32*, 327−338.

BI051893G